Kishal Bipin Tandel
23MS115

Report 1

August 24, 2025

PH3105: Nuclear Physics Laboratory

Abstract

In this experiment, We used radioactive ^{22}Na as a source of γ ray photons. We first determined the linear attenuation coefficient, mass attenuation coefficient and half value thickness of aluminium and then verified the inverse square law of radiation for γ ray photons.

Contents

1. Introduction

1.1 Aim

1. To determine linear and mass attenuation coefficients and half value thickness of aluminium.

2. To verify inverse square law of radiation for γ ray photons.

1.2 Apparatus

The source of γ-ray photons in this experiment is a radioactive ^{22}Na source. The emitted radiation is detected using a Geiger–Müller (GM) tube, which is connected to a GM counter for pulse counting. The data acquisition is carried out through the software *Measure*, provided by the lab's instrumentation system, which recorded the GM counter's pulse rates in real time. Additional experimental setup includes an absorber (aluminium slab) holder and a source holder with adjustable distance for inverse square law verification.

1.3 Experimental Set-up

The experimental set-up is shown in Figure 1.
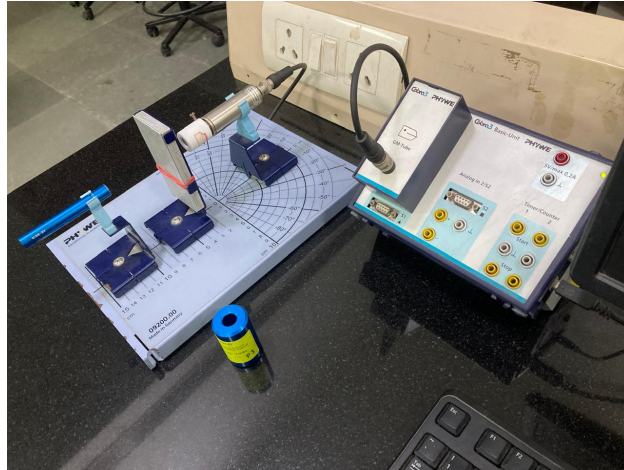
Figure 1: Experimental set-up

2. Theory

2.1 Functioning of Geiger-Müller Counter

A schematic of the Geiger-Müller counter is shown in Figure 2.

When an ionizing radiation passes through the gas in an ionizing chamber, it produces a few ions by knocking off an electron from the argon atoms. If the applied potential difference is strong enough, these ions will produce a secondary ion avalanche whose total effect will be proportional to the energy associated with the primary ionizing event.

The operation of the counter depends on the formation of Townsend avalanches within the gas of the counter tube. As little as one pair of ions is sufficient to trigger the counter. These primary

Figure 2: Schematic diagram of a Geiger-Müller counter setup.

ions begin to move under the influence of the electric field, the positives going to the tube and the negatives, largely electrons, moving in the direction of the center wire. Thus the electrons move into the region of the rapidl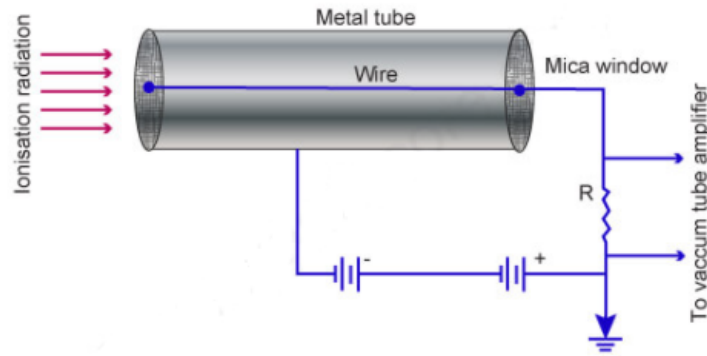y increasing electric field where they soon acquire sufficient energy to produce additional ions by collisions with neutral argon atoms. The positive ions move much more slowly because of their greater mass, and therefore do not produce significant amount of secondary ions. As each new generation of electrons is produced it, in turn, acquires sufficient energy to ionize the gas as it moves toward the wire. The result is great amplification of the primary ionization by the time this electrical disturbance reaches the wire. The amplification in this process is of the order of 10^9.

The description of the process that produces a pulse outlined above implies that a certain minimum potential is required across the counter before it will operate as a Geiger-Muller counter. This is the potential at which electron avalanches begin to form. Above this potential the size of the individual pulses will grow with the increase of voltage, but the number of pulses per second for a constant source of radiation should, on the average, remain practically constant. This condition should continue until the voltage reaches a point where the shielding effect of the positive ion sheath begins to break down and a continuous discharge across the counter can be set up. This prediction is verified in the curve shown in Figure 3. In this graph the counting rate is plotted along the y-axis and the potential across the counter along the x-axis. This data is taken with a constant source of radiation and reveals the effect of the increase in potential on the operation of the counter. The value of the voltage at which counting begins is called the starting voltage. In some cases this has been defined as the extrapolated intersection of the rising curve back to the x-axis. This helps to avoid the ambiguity in the determination of the point at which counting starts. This point is actually a function, to some extent, of the sensitivity of the detecting circuit. The nearly horizontal part of this curve, called the plateau, represents the possible working range. If the source of potential for the counter is somewhat variable, it is usually advisable to select the middle of the plateau as the mean value of the voltage applied to the counter. The slope of this plateau in a good counter is not over 2 to 5 percent per hundred volts over a region of the order of 200 volts. The actual slope sets the limit of the permissible fluctuation in the high voltages for a given accuracy of measurement.

The threshold voltage of the Geiger counter is defined as the voltage across the counter at which the Geiger action begins. As has been mentioned, in this region the pulses for a given voltage are uniform in height. The threshold is usually greater than the starting voltage, and the difference between it and the starting voltage depends in part on the sensitivity of the equipment used for detecting the pulses. As has been indicated, counters are operated, corresponding to some point on
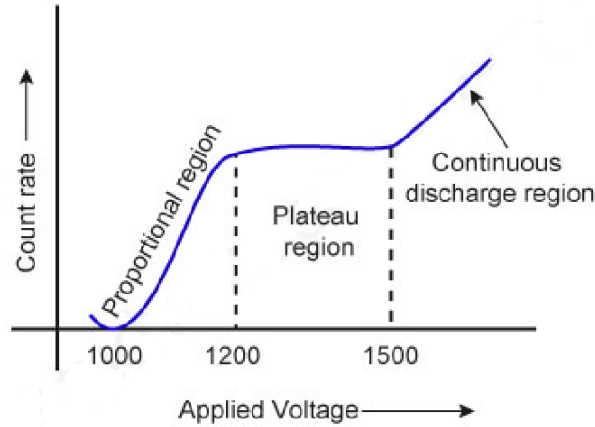
Figure 3: Count Rate vs Applied Voltage plot

the plateau, at a voltage in excess of the threshold voltage. This excess is called the over-voltage. The magnitude of the pulses increases with the over-voltage.

In the Geiger region, which occurs when the potential applied across the counter, in relation to the dimensions of the center wire and tube as well as the gas pressure, are appropriately chosen, all pulses are closely of the same size for a given voltage regardless of the number of primary ions that initiated the pulse. This is a natural result of the large gas amplification obtained in the electron avalanche type of discharge. When the avalanche has reached it, the wire suffers a sudden change of potential as the result of the removal of the positive ions from the vicinity of the wire by the strong electric field in this region. This change of potential is in the direction of lowering the potential difference across the tube. The resistor connected to the center wire has a high value, so that this reduction of potential persists for a measurable time. This process results in the interruption of the electrical discharge and the termination of the counting operation. The resistor permits the charge to leak off the central wire, thus restoring the counter to its initial condition, ready to record another count. If the resistor did not have a value of the order of 10^9 ohms, a continuous discharge would tend to form in the counter tube, fed by electrons released from the walls of the tube by the impact of the positive ions. This situation is characteristic of all counters using a permanent gas for filling. These counters are also slow counters due to their long recovery time. This time is related to the value of RC where R is the 10^9 ohm resistor, and C is the capacity of the wire system. This capacity is usually of the order of 10^{-11} farad. Therefore, RC is equal to 0.01 sec, being the time required for the wire to fall to $1/e$ of the maximum charge in its potential. Ions formed in the counter at intervals less than 0.01 sec apart could hardly be expected to produce clearly defined separate pulses in the counter.

2.2 Linear and Mass Attenuation Coefficients

Linear attenuation coefficient μ is the probability per unit path length that a photon will interact with the material. It depends on material's density ρ and its composition. So denser materials (lead, iron) have larger μ than lighter ones (aluminium, plastic).

Mass attenuation coefficient is linear attenuation coefficient divided by material's density ρ i.e., it is equal to μ/ρ. It normalizes attenuation to the mass of material per unit area rather than thickness. Mass attenuation coefficient is an intrinsic property of the material at a given photon

4

energy, independent of density or state. This makes it easier to compare different absorbers or tabulate values.

Now let us derive the functional equation for determining the linear attenuation coefficient μ (and hence mass attenuation coefficient ρ). Let I_0 be the γ ray intensity incident on the metal slab. Let I be the emergent intensity of γ ray photons after passing through the slab. Let the thickness of the metal slab be t. The change in intensity dI at any time is directly proportional to the intensity at that time. Also the intensity will decrease as the thickness t of the slab increases because γ ray photons have a pass through more material which increases the probability of the photons getting absorbed by the material. Thus using these facts, we can write:

$$dI \propto -Idt$$
$$\Rightarrow \quad dI = -\mu I dt$$
$$\Rightarrow \quad \int_{I_0}^{I} \frac{dI}{I} = -\mu \int_{0}^{t} dt$$
$$\Rightarrow \quad \ln \left| \frac{I}{I_0} \right| = -\mu t$$
$$\Rightarrow \quad \boxed{\ln |I| = -\mu t + \ln |I_0|} \tag{2.2.1}$$
$$\Rightarrow \quad \boxed{I = I_0 e^{-\mu t}} \tag{2.2.2}$$

In Eqs. (2.2.1) and (2.2.2), I_0 and I are the incident and emergent intensity (or count rate) respectively of the γ ray photons, t is the thickness of the metal slab and μ is the linear attenuation coefficient. Thus using Eq. (2.2.1), we can calculate linear attenuation coefficient μ and mass attenuation coefficient μ/ρ.

2.3 Half Value Thickness HVT

Half value thickness $t_{\frac{1}{2}}$ for an absorber is its thickness, traversing through which, the radiation's intensity becomes half of its incident intensity. Using Eq. (2.2.1) at half value thickness (i.e., when $I/I_0 = 0.5$), we have:

$$\boxed{t_{\frac{1}{2}} = \frac{\ln |2|}{\mu}} \tag{2.3.1}$$

2.4 Inverse Square Law of Radiation

Since a point source emits radiation spherically in all directions and since the area of a sphere ($A = 4\pi r^2$) increases as r^2, the intensity, which is power per unit area, decreases as $1/r^2$. Therefore, we have:

$$I = \frac{C}{r^2} \qquad \qquad \text{(C is a constant)}$$
$$\Rightarrow \quad \boxed{\ln |I| = -2 \ln |r| + C'} \qquad \text{(C' is a constant)} \tag{2.4.1}$$

In Eq. (2.4.1), I is the incident intensity (or count rate) of the γ ray photons and r is the distance between source and detector. Thus using Eq. (2.4.1), we can verify the inverse square law of radiation for γ ray photons.

2.4 Decay Scheme of ^{22}Na

The modes of decay are listed below:

1. Positron emission (β^+-decay):

$$^{22}_{11}\text{Na} \longrightarrow {}^{22}_{10}\text{Ne}^* + e^+ + \nu_e \tag{2.5.1}$$

2. Electron capture (EC):

$$^{22}_{11}\text{Na} + e^- \longrightarrow {}^{22}_{10}\text{Ne}^* + \nu_e \tag{2.5.2}$$

In Eqs. (2.5.1) and (2.5.2), $^{22}_{10}\text{Ne}^*$ is the excited state of neon-22, e^+ is the positron, e^- is the electron, and ν_e is the electron neutrino. In both cases, the daughter nucleus $^{22}_{10}\text{Ne}^*$ is left in an excited state, which de-excites to its ground state by emitting a γ-ray photon of energy $E_\gamma = 1.275$ MeV.

The emitted positron (e^+) from β^+-decay interacts with an electron (e^-) in the surrounding medium, leading to annihilation:

$$e^+ + e^- \longrightarrow 2\gamma$$
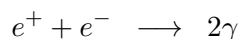
This produces two back-to-back γ-rays, each of energy $E_\gamma = 0.511$ MeV.

3. Determination of Background Inetnsity

Due to the presence of background intensity in the laboratory, we first find the mean count rate for background intensity photons. We have taken each reading for 300 seconds.

Count (per 300 s)	Count Rate (s^{-1})	Mean Count Rate (s^{-1})
107	0.36	
111	0.37	0.36
106	0.35	

Table 1: Determination of background intensity.

4. Determination of Attenuation Coefficients and HVT of Al

4.1 Determination of Incident Intensity I_0

We have taken each reading for 90 seconds. After calculating mean count rate, we will subtract the mean background count rate from it to get corrected incident count rate I_0.

Count (per 90 s)	Count Rate (s^{-1})	Mean Count Rate (s^{-1})	Corrected Incident Count Rate I_0 (s^{-1})
60	0.67		
64	0.71	0.69	0.33
62	0.69		

Table 2: Determination of incident intensity.

4.2 Observation Table

We have taken each reading for 90 seconds. After calculating mean count rate, we will subtract the mean background count rate from it to get corrected count rate I.

Sr. No.	Thickness t (in mm)	Count (per 90 s)	Count Rate (s^{-1})	Mean Count Rate (s^{-1})	Corrected Count Rate I (s^{-1})
1	0.99	65 59 61	0.72 0.66 0.68	0.69	0.33
2	2.03	61 58 60	0.68 0.64 0.67	0.66	0.30
3	3.02	61 60 61	0.68 0.67 0.68	0.68	0.32
4	4.00	62 57 58	0.69 0.63 0.64	0.65	0.29
5	5.08	61 58 59	0.68 0.64 0.66	0.66	0.30
6	6.61	60 59 56	0.67 0.66 0.62	0.65	0.29
7	6.71	58 55 59	0.64 0.61 0.66	0.64	0.28
8	10.48	56 54 57	0.62 0.60 0.63	0.62	0.26
9	10.71	57 58 55	0.63 0.64 0.61	0.63	0.27
10	11.56	54 59 53	0.60 0.66 0.59	0.62	0.26
11	12.54	53 58 54	0.59 0.64 0.60	0.61	0.25
12	13.53	56 54 53	0.62 0.60 0.59	0.60	0.24

Sr. No.	Thickness t (in mm)	Count (per 90 s)	Count Rate (s^{-1})	Mean Count Rate (s^{-1})	Corrected Count Rate I (s^{-1})
13	14.57	51	0.57	0.60	0.24
		57	0.63		
		53	0.59		
14	15.56	55	0.61	0.60	0.24
		56	0.62		
		51	0.57		
15	15.74	55	0.61	0.61	0.25
		54	0.60		
		56	0.62		

Table 3: Observation Table: Thickness t vs Count Rate I

4.3 Data Analysis and Plotting

Using Eq. (2.2.1), if we plot $\ln|I|$ vs. t, we get a straight line as shown in Figure 4.
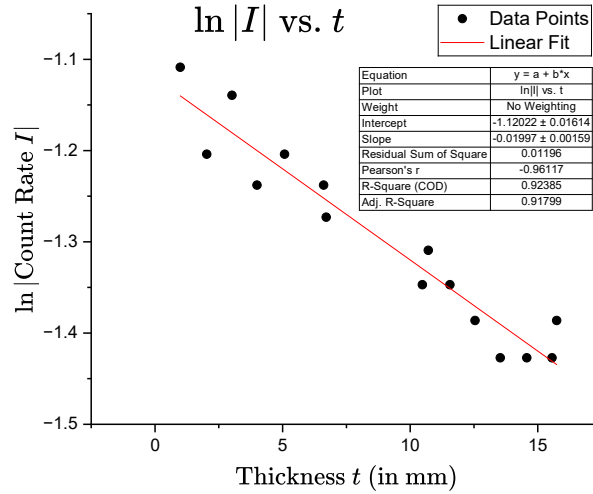
Figure 4: $\ln|I|$ vs. t plot

The slope of this plot is -0.01997 mm^{-1} and the y-intercept is -1.12022. Using Eq. (2.2.1), we get:

$$\ln|I_0| = -1.12022$$

$$\Rightarrow \quad \boxed{I_0 \approx 0.33 \text{ s}^{-1}} \tag{4.3.1}$$

Eq. (4.3.1) tells the count rate of incident γ ray photons reaching the detector when there is no absorber in its path. This value of incident count rate is the same as we experimentally found in Table 2.

4.4 Calculation

Using Eq. (2.2.1) and using the slope of Figure 4, the linear attenuation coefficient μ of aluminium is:

$$\boxed{\mu = 0.01997 \text{ mm}^{-1}} \tag{4.4.1}$$

The literature value of density ρ of aluminium is 2.7 g/cm^3 =2.7 mg/mm^3. Therefore the value of the mass attenuation coefficient of aluminium is given by:

$$\boxed{\frac{\mu}{\rho} = \frac{0.01997}{2.7} \approx 7.39630 \times 10^{-3} \text{ mm}^2\text{mg}^{-1}} \tag{4.4.2}$$

Substituting $\mu = 0.01997$ mm^{-1} in Eq.(2.3.1), we get the half value thickness $t_{\frac{1}{2}}$ for aluminium as:

$$t_{\frac{1}{2}} = \frac{\ln|2|}{0.01997}$$
$$\Rightarrow \quad \boxed{t_{\frac{1}{2}} = 34.70942 \text{ mm}} \tag{4.4.3}$$

5. Verification of Inverse Square Law of Radiation

5.1 Observation Table

We have taken each reading for 90 seconds. After calculating mean count rate, we will subtract the mean background count rate from it to get corrected count rate I.

Sr. No.	Distance r (in cm)	Count (per 90 s)	Count Rate (s^{-1})	Mean Count Rate (s^{-1})	Corrected Count Rate I (s^{-1})
1	1.5	3642	40.47	40.46	40.10
		3633	40.37		
		3649	40.54		
2	2.0	2294	25.49	25.52	25.16
		2299	25.54		
		2297	25.52		
3	2.5	1425	15.83	15.90	15.54
		1433	15.92		
		1435	15.94		
4	3.0	919	10.21	10.24	9.88
		917	10.19		
		930	10.33		
5	3.5	690	7.67	7.70	7.34
		697	7.74		
		693	7.70		
6	4.0	592	6.58	6.63	6.27
		601	6.68		
		597	6.63		

Sr. No.	Distance r (in cm)	Count (per 90 s)	Count Rate (s^{-1})	Mean Count Rate (s^{-1})	Corrected Count Rate I (s^{-1})
7	4.5	434	4.82	4.89	4.53
		437	4.86		
		449	4.99		
8	5.0	361	4.01	4.04	3.68
		362	4.02		
		369	4.10		
9	5.5	340	3.78	3.73	3.37
		337	3.74		
		331	3.68		
10	6.0	285	3.17	3.21	2.85
		294	3.27		
		288	3.20		
11	6.5	252	2.80	2.80-	2.44
		250	2.78		
		254	2.82		
12	7.0	209	2.32	2.35	1.99
		210	2.33		
		217	2.41		
13	7.5	175	1.94	1.95	1.59
		174	1.93		
		179	1.99		
14	8.0	165	1.83	1.87	1.51
		167	1.86		
		173	1.92		
15	8.5	159	1.77	1.79	1.43
		164	1.82		
		161	1.79		
16	9.0	142	1.58	1.60	1.24
		147	1.63		
		143	1.59		
17	9.5	139	1.54	1.50	1.14
		134	1.49		
		133	1.48		
18	10.0	125	1.39	1.36	1.00
		119	1.32		
		123	1.37		

Table 4: Observation Table: Distance r vs Count Rate I

5.2 Data Analysis and Plotting

Using Eq. (2.4.1), if we plot $\ln|I|$ vs. $\ln|r|$, we get a straight line as shown in Figure 5.

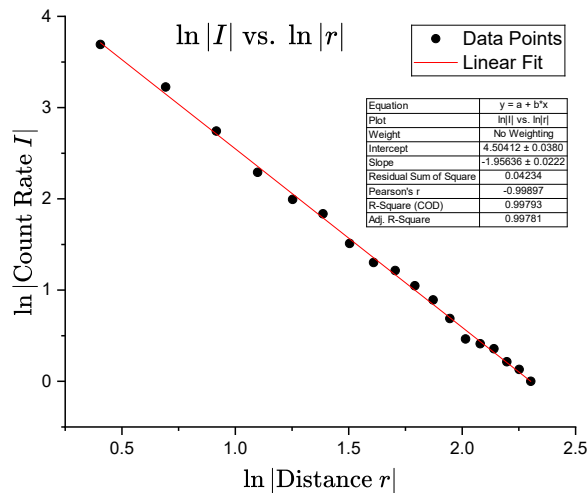

Figure 5: $\ln|I|$ vs. $\ln|r|$ plot

The slope of this plot is -1.95636 and the y-intercept is 4.50412. As evident using Eq. (2.4.1), γ ray photons do follow inverse square law of radiation since the slope of this plot is very close to -2.

5.3 Error Analysis

1. Absolute Error δ:

$$\delta = \frac{|\text{Literature Value-Experimental Value}|}{\text{Literature Value}} = \frac{|2 - 1.95636|}{2} = 0.02182$$

2. Fractional/Relative Error ϵ:

$$\epsilon = \frac{\text{Absolute Error } \delta}{\text{Literature Value}} = \frac{0.02182}{2} = 0.01091$$

3. Percentage Error η:

$$\eta = \text{Relative Error } \epsilon \times 100\% = 0.01091 \times 100\% = 1.091\%$$

6. Sources Of Error

6.1 Systematic Errors

1. **Calibration error:** The Geiger-Müller counter calibration may have slight offsets, leading to inaccurate count rate measurements.

2. **Absorber thickness or roughness uncertainty:** Non-uniform thickness or surface roughness of aluminium slabs introduces deviation in attenuation measurements.

3. **Source strength variation:** Decay of the γ-ray source over time introduces a systematic decrease in count rate.

4. **Geometrical misalignment:** Imperfect alignment of source, absorber, and detector changes effective path length of radiation.

5. **Finite source size:** The γ-ray source is not a perfect point source. Its finite dimensions introduce deviations from the ideal inverse square law.

6. **Dead time of GM counter:** The counter has a finite dead time; during this period after each detection, further events are not registered, leading to undercounting at higher count rates.

6.2 Random Errors

1. **Fluctuating background radiation:** Though we accounted for the background intensity in our readings, if it fluctuates too much from the measured mean value, it can introduce significant errors.

2. **Electronic fluctuations:** Random pulses due to electronic interference may have contributed to variations in recorded counts.

3. **Environmental factors:** Variations in temperature, pressure, and humidity can affect detector efficiency and introduce error in measurements.

7. Results

In this experiment, we determined the following values:

1. Linear attenuation coefficient of aluminium, $\mu = 0.01997$ mm^{-1}

2. Mass attenuation coefficient of aluminium, $\dfrac{\mu}{\rho} = 7.39630 \times 10^{-3}$ mm^2 mg^{-1}

3. Half value thickness of aluminium, $t_{\frac{1}{2}} = 34.70942$ mm

4. Relationship between intensity of γ ray photon and distance: $I \propto r^{-1.95636}$

8. Conclusion

The experiment successfully demonstrated the absorption of γ-rays in matter and validated the exponential attenuation law as given by Eq. (2.2.2).

1. Using aluminium as absorber, the linear attenuation coefficient, mass attenuation coefficient, and half-value thickness were determined.

2. The inverse square law of radiation was verified within experimental limits, with minor deviations attributed to absorption in air and scattering.

Overall, the experimental values were in reasonable agreement with theoretical expectations.

Future extensions of this work could include repeating the experiment with different absorbers (Pb, Fe), verifying the energy dependence of attenuation and verifying the inverse square law of radiation at large distance by accounting for scaterring and absorption by air molecules. However, these were beyond the present scope.

References

[1] G. F. Knoll, *Radiation Detection and Measurement*, 4th ed., Wiley, 2010.

[2] A. Beiser, *Concepts of Modern Physics*, 6th ed., McGraw–Hill, 2003.